JOURNAL OF GUIDANCE, CONTROL, AND DYNAMICS
Vol. 27, No. 6, November–December 2004

Dynamic Lateral Entry Guidance Logic

Zuojun Shen* and Ping Lu†
Iowa State University, Ames, Iowa 50011-2271

Lateral motion of an entry vehicle is controlled by the sign of its bank angle, determined by the entry guidance system. The conventional technique for changing the bank sign is based on prespecified threshold values in the heading error of the vehicle with respect to the landing site. A new automated lateral guidance logic is developed based on the crossrange, which is found to be a more suitable parameter than the heading error for lateral guidance. The present guidance logic determines the bank reversals by constantly evaluating information from the reference crossrange profile, current crossrange, and estimated actual lift-to-drag ratio. Near the end of the trajectory, a noniterative numerical predictor decides whether a final bank reversal is needed to null the heading error. This algorithm enables the entry guidance system to fly a wide range of missions and vastly different bank-angle profiles and provides reliable and good performance in the presence of significant aerodynamic modeling uncertainty. All of these tasks can be accomplished without requiring manual tuning of guidance parameters or using an excessive number of bank reversals. Extensive high-fidelity simulations with different mission scenarios and significant dispersions are presented to demonstrate the performance of the proposed method.

I. Introduction

THE entry guidance system for a lifting entry vehicle controls the bank angle and angle of attack during the atmospheric flight from the entry interface at about altitude 120 km until the velocity decreases to Mach 2–3 (Ref. 1). The guidance commands are generated by tracking a reference trajectory which is designed either in preflight planning,[1] or potentially on board, as recent efforts have attempted to achieve.[2–4] In the traditional approach, the reference to be tracked represents the desired longitudinal profiles as in the case of the shuttle, where the reference is a drag-acceleration-vs-velocity profile that equivalently defines the range-vs-energy condition.[1] Tracking the longitudinal profiles determines the magnitude of the bank-angle command. The sign of the bank-angle command, on the other hand, is changed to the opposite whenever the heading error with respect to the targeted landing site exceeds a prespecified threshold. This forced change of bank sign is referred to as bank-angle reversal. The traditional approach works well when the actual flight goes as planned in pre-mission analysis and the actual bank-angle magnitude remains close to the reference value. When the bank profile flown is significantly different, the bank-reversal threshold criterion will require adjustments, typically made through simulations. The situations where a very different bank-angle profile may be necessary include entry from a different orbit, landing at an alternate landing site, variations in entry conditions leading to much different downrange and crossrange, and contingency entry missions (such as on-demand entry and aborts) that are not planned. The recent advances in trajectory-planning algorithms would potentially allow on-board generation of a reference trajectory based on the actual conditions. However, the corresponding bank-angle profiles could be drastically different from the nominal one. Similar situations can develop in the presence of significant aerodynamic modeling mismatch, where flying even the nominal longitudinal profiles may necessitate a bank-angle profile considerably different from the nominal bank profile. In these cases, the use of the predefined bank-reversal threshold could sometimes result in a total miss of the landing site (see the example in Sec. III.A and simulation results in Sec. VI.C).

Some recent research efforts employ simultaneous tracking of longitudinal and lateral reference profiles.[5] In this approach both the sign and the magnitude of the bank angle are determined by the tracking law, and there is no need for additional bank-reversal logic. These features make this approach appealing when used in conjunction with an on-board trajectory-planning algorithm. For vehicles with medium or higher lift-to-drag (L/D) ratios, methods of this type can work satisfactorily.[6] But practical difficulty arises for vehicles with low L/D values, and even for vehicles with medium L/D ratios that have large aerodynamic modeling uncertainty. The reason is that with low lifting capability, the vehicle dynamics simply do not simultaneously admit the reference profiles in both longitudinal and lateral directions in the presence of trajectory dispersions and/or aerodynamic modeling mismatch. Consequently the vehicle cannot follow the planned longitudinal and lateral profiles at the same time. The manifestation of this incompatibility is that the tracking performance will be very poor regardless of how the tracking law is designed or tuned. The same phenomenon will occur with vehicles that have moderate lifting capability but significant aerodynamic-modeling mismatch (such as new test vehicles). Indeed, this is probably the reason that the performance of three-dimensional linear–quadratic regulator (LQR) tracking laws never matches the performance achieved by longitudinal LQR-based tracking laws, as shown in Ref. 7. In these cases it appears clear that the guidance law should focus on tracking only the reference longitudinal profile because most of the critical trajectory parameters such as range, energy, and path-constraint observance are only concerned with longitudinal motion. The reference lateral profiles do not have to be tightly tracked, as long as the required final heading condition is met by choosing the proper sign of the bank angle. This strategy would leave adequate margin for the bank angle to accommodate longitudinal trajectory dispersions. While the value of the classical shuttle entry guidance principle is being "rediscovered," the contribution of this paper is the development of new automated lateral entry guidance logic that fully addresses the needs and issues raised in the preceding paragraph.

A key difference between the proposed method and the shuttle-type bank-reversal logic is the use of current crossrange instead of heading error in the determination of when to perform bank reversals. The crossrange is found to be a nearly linear parameter more slowly varying than the heading error, especially toward the later part of the trajectory. A chief challenge in the design of the bank-reversal logic is to ensure in all cases that the trajectory will not

Received 1 February 2004; revision received 12 April 2004; accepted for publication 12 April 2004; presented as Paper 2004-4773 at the AIAA Guidance, Navigation, and Control Conference, Providence, RI, 16–19 August 2004.

*Postdoctoral Research Associate, Department of Aerospace Engineering, 2271 Howe Hall.

†Professor, Department of Aerospace Engineering, 2271 Howe Hall; plu@iastate.edu. Associate Fellow AIAA.

miss the turn and lose the chance for safe landing. Yet unnecessary bank reversals should be avoided. To account for the profound impact of large but slowly varying aerodynamic modeling errors on the lateral motion of the entry vehicle, the bank-reversal decision also incorporates the on-board-estimated difference between the actual value of L/D and its modeled value. Near the end of the trajectory, numerical integration is used to determine when a last bank reversal is needed to guarantee small final heading error. This is a safeguard that is responsible for the ensured high precision in the final heading condition yielded by this method. These dynamically adjusted steps in this lateral guidance logic contrast with the more passive shuttle-based bank reversal logic. To ensure that the lateral guidance logic functions as desired, the precision of the longitudinal tracking must be good. It is found that a combined proportional-plus-integral control law that blends standard energy-scheduled gains and constant gains provides remarkably better and more consistent longitudinal-tracking performance than either of the individual set of gains can achieve. Extensive numerical testing in a high-fidelity simulation environment has been carried out to validate the proposed entry-guidance design. The comparison of the performance with that of the conventional approach in the same test cases offers convincing support for the stronger capability of the current entry guidance method.

II. Entry Guidance Problem Formulation

A. Dynamics

For entry guidance design purposes, rotating-Earth effects are not important and can be easily compensated for by the feedback nature of the guidance laws. Thus the three-degree-of-freedom (3DOF) dynamics of an entry vehicle over a nonrotating spherical Earth are described by the following dimensionless equations of motion:

$$\dot{r} = V \sin\gamma \tag{1}$$

$$\dot{\theta} = \frac{V \cos\gamma \sin\psi}{r \cos\phi} \tag{2}$$

$$\dot{\phi} = \frac{V \cos\gamma \cos\psi}{r} \tag{3}$$

$$\dot{V} = -D - \frac{\sin\gamma}{r^2} \tag{4}$$

$$\dot{\gamma} = \frac{1}{V}\left[L\cos\sigma + \left(V^2 - \frac{1}{r}\right)\left(\frac{\cos\gamma}{r}\right)\right] \tag{5}$$

$$\dot{\psi} = \frac{1}{V}\left[\frac{L\sin\sigma}{\cos\gamma} + \frac{V^2}{r}\cos\gamma\sin\psi\tan\phi\right] \tag{6}$$

where r is the radial distance from the center of the Earth to the vehicle, normalized by the radius of the Earth, $R_0 = 6{,}378{,}135$ m. With slight abuse of terminology, r is sometimes referred to as "altitude" in this paper. The longitude and latitude are θ and ϕ, respectively. The Earth-relative velocity V is normalized by $V_c = \sqrt{(g_0 R_0)}$ with $g_0 = 9.81$ m/s^2. The terms D and L are the aerodynamic drag and lift accelerations in g; that is, $D = \rho(V_c V)^2 S_{\text{ref}} C_D/(2mg_0)$ and $L = \rho(V_c V)^2 S_{\text{ref}} C_L/(2mg_0)$, where ρ is the atmospheric density and S_{ref} the reference area of the vehicle, and m the mass of the vehicle. Note that D and L are also functions of α, the angle of attack, through the dependence of the drag and lift coefficients C_D and C_L on α. The relative flight path angle is γ and σ is the bank angle. The relative-velocity azimuth angle ψ is measured from the north in a clockwise direction. The differentiation is with respect to the dimensionless time $\tau = t/\sqrt{(R_0/g_0)}$.

The longitudinal state variables are r, V, and γ. Note that the longitudinal state equations are decoupled from the lateral state variables, and only the magnitude of σ affects the longitudinal dynamics.

B. Entry Guidance Problem

The entry guidance problem is to determine the required bank-angle σ and angle-of-attack α commands that steer the vehicle throughout entry flight phase. The entry flight ends at the terminal-area-energy-management (TAEM) interface for horizontal landing. In this paper, the term "TAEM" will be used in a generic sense so that it refers to the termination of entry flight, regardless of whether glide landing or parachute landing ensues. At the TAEM point, the entry trajectory must have correct conditions. These requirements form the terminal conditions for the entry trajectory, typically in the form of

$$r_f = r_{\text{TAEM}} \tag{7}$$

$$V_f = V_{\text{TAEM}} \tag{8}$$

$$s_f = s_{\text{TAEM}} \tag{9}$$

where s_f is the final value of range-to-go s_{togo}, defined to be the range from the vehicle position to a target point. For horizontal landing this would be the center of the heading-alignment cone (HAC) near the end of the runway. Again the term "HAC" will be cited in a generic sense in this paper. For parachute landing, HAC will simply mean the landing site. The coordinates of the HAC, $(\theta_{\text{HAC}}, \phi_{\text{HAC}})$, are known. The TAEM altitude r_{TAEM}, velocity V_{TAEM}, and range to HAC s_{TAEM} are all specified for a given vehicle. In addition, the Earth-relative velocity vector at the TAEM interface should be pointing nearly to the HAC. Let $\Delta\psi = \psi - \psi_{\text{LOS}}$, where ψ_{LOS} is the azimuth angle of the great circle containing the HAC and the vehicle at the vehicle's current location (or the angle between the north and the line of sight from the vehicle to the HAC when the curvature of the Earth's surface is ignored). The condition of final heading alignment on $\Delta\psi_f$ is then represented by

$$|\Delta\psi_f| \le \Delta\psi_{\text{TAEM}} \tag{10}$$

for a preselected $\Delta\psi_{\text{TAEM}} \ge 0$. This condition stipulates that the final velocity vector should be directed at the HAC within a given tolerance $\Delta\psi_{\text{TAEM}}$. This is an important condition for approach/landing in the case of horizontal landing vehicles. For a vertical landing vehicle, this condition is implicitly enforced by the requirement that the vehicle arrive at the landing site (where at the last moment $\Delta\psi$ has no definition).

The entry trajectory is also constrained by a number of path constraints for thermal protection, load, and vehicle integrity considerations. Examples of the path constraints are heat rate, normal aerodynamic-load factor, and dynamic pressure, as expressed in the following:

$$\dot{Q} \le \dot{Q}_{\max} \tag{11}$$

$$|L\cos\alpha + D\sin\alpha| \le n_{z_{\max}} \tag{12}$$

$$\bar{q} \le \bar{q}_{\max} \tag{13}$$

where $\bar{q} = \rho V^2/2$, and the heat rate is represented by

$$\dot{Q} = k\sqrt{\rho}V^{3.15} \tag{14}$$

with a constant k. The values of $\dot{Q}_{\max}$, $n_{z_{\max}}$, and $\bar{q}_{\max}$ are all specified. Additional constraints may include those on temperatures at various body points and on equilibrium glide conditions. Depending on the vehicle configuration and whether crew is aboard, the body-normal load constraint (12) may be replaced by the total load constraint,

$$\sqrt{L^2 + D^2} \le n_{\max} \tag{15}$$

A basic assumption in this paper is that a complete 3DOF reference trajectory is available, containing the histories of all six state variables in Eqs. (1–6) and the corresponding σ and α. All of these targeting conditions and path constraints are taken into consideration in the design of the reference trajectory. The information in the reference lateral profiles will be used in determining bank reversals. The guidance law will track the reference longitudinal profiles. In

particular, the primary variable to be tracked is the dimensionless range-to-go to HAC, given in radians along a great circle:

$$s_{\text{togo}} = \cos^{-1}[\sin\phi_{\text{HAC}}\sin\phi + \cos\phi_{\text{HAC}}\cos\phi\cos(\theta_{\text{HAC}} - \theta)] \quad (16)$$

Because 1 deg of arc length taken along a great circle on the surface of the spherical Earth is equal to 111.12 km (60 nm), the value of s_{togo} is sometimes cited in units of distance (kilometers) in the subsequent sections for the convenience of the reader.

The independent variable used in the guidance is (the negative of) the dimensionless specific energy, defined to be

$$e = 1/r - V^2/2 \quad (17)$$

Based on the time derivatives of s_{togo} and e, it can be easily shown that with the approximation $\Delta\psi \approx 0$ we have

$$\frac{\mathrm{d}s_{\text{togo}}}{\mathrm{d}e} = -\frac{\cos\gamma}{rD} \quad (18)$$

Because the derivative of s_{togo} is dependent only on longitudinal state variables, s_{togo} is considered a longitudinal variable.

III. Lateral Motion

A. Conventional Bank-Reversal Logic

The conventional bank-reversal criterion is based on whether the condition

$$|\Delta\psi| \le \Delta\psi_{\text{threshold}} \quad (19)$$

is observed. If not, the sign of the bank angle is set to the opposite of the sign of the current heading error, and this sign is maintained until Eq. (19) is again violated. The threshold value $\Delta\psi_{\text{threshold}}$, which is usually chosen to be a piecewise constant or linear function of the relative velocity, is designed so that when the entry trajectory ends, the final heading condition Eq. (10) is met. The selection of a proper $\Delta\psi_{\text{threshold}}$ will depend on the magnitude of the bank-angle profile, which is determined by tracking the longitudinal profile, and to some extent on the crossrange of the entry mission as well. The dependence on the magnitude of the bank angle is easy to understand: a larger bank angle results in more heading changes, and a larger $\Delta\psi_{\text{threshold}}$ is appropriate to avoid an excessive number of bank reversals. On the other hand, a smaller magnitude of the bank angle produces fewer changes in the heading; thus a tighter $\Delta\psi_{\text{threshold}}$ will be necessary to ensure the final heading condition, condition (10). When the crossrange differs significantly from mission to mission, $\Delta\psi_{\text{threshold}}$ may also need to be adjusted even if the longitudinal profile remains approximately the same. In all cases the adjustments are done by inspecting the simulation results and changing the parameters defining $\Delta\psi_{\text{threshold}}$ accordingly.

For a fully autonomous entry guidance system that can adapt to various mission scenarios including unplanned events, an on-board trajectory-planning capability, along with an automated tracking-guidance approach, will be required. Although substantial strides have been made toward the former,[2–4] automated bank-reversal logic is the remaining key to the latter, because longitudinal profile tracking can now be satisfactorily handled (cf. Ref. 7 and Sec. V in this paper). In a recent effort, Ref. 8 presents a bank-reversal-management logic that determines where to place the bank reversal(s) in reference trajectory update based on the current information. The approach taken in this paper is to provide the guidance logic with the ability to adjust. A dynamically adjusted lateral guidance logic could make a dramatic difference in the presence of significant aerodynamic modeling inaccuracy, even if the vehicle is to fly a preplanned mission. For example, when the actual lift coefficient is less than the modeled value, the longitudinal-tracking law will use a bank-angle profile of magnitude smaller than that of the nominal bank angle. If this difference becomes sufficiently large, the vehicle could lack adequate turning capability after a bank reversal that is determined on the basis of the nominal profiles. As a result, the vehicle could miss the HAC completely by making the bank reversal too late.

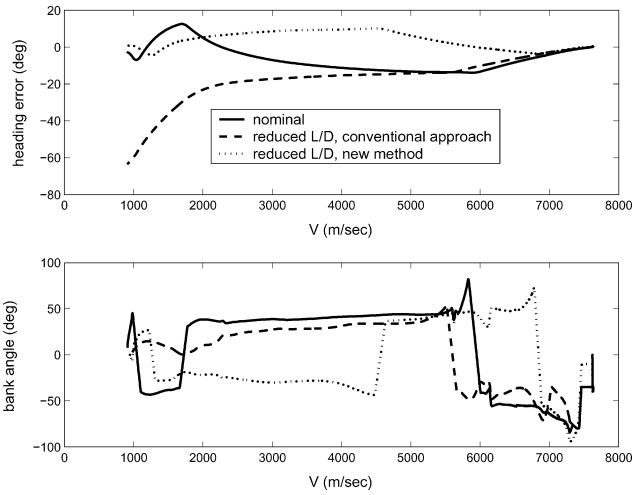

Fig. 1 Heading errors and bank angles for X-33 in the nominal case and with a −20% dispersion in *L/D*.

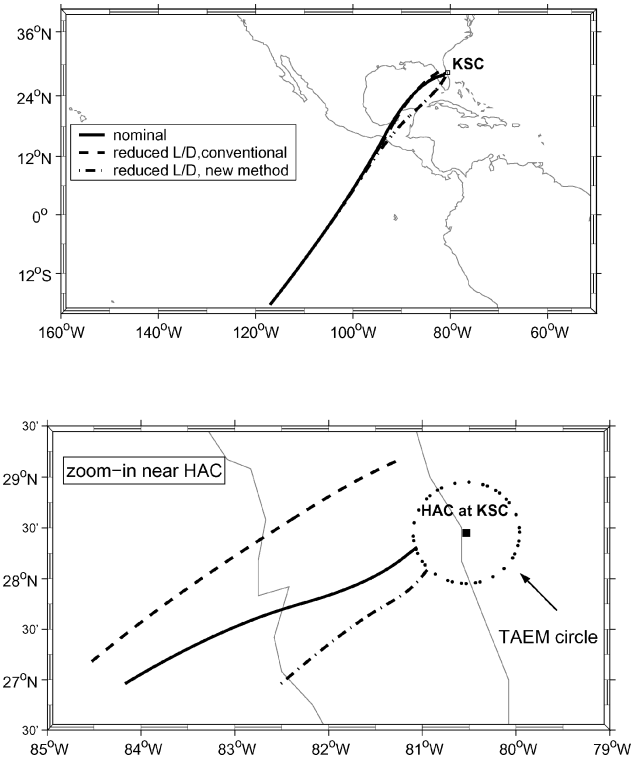

Fig. 2 Ground tracks and their zoom-in views for X-33 in the nominal case and with a −20% dispersion in *L/D*.

Figures 1 and 2 show such an example. The vehicle model is of the X-33, a half-scale prototype of a reusable launch vehicle design with a lifting-body configuration. The mission is an entry flight returning from the International Space Station orbit and landing horizontally at the Kennedy Space Center (KSC). The TAEM interface is defined by the TAEM velocity V_{TAEM} corresponding to Mach 3. The range-to-HAC at the TAEM interface, s_{TAEM}, is specified to be 55.6 km (30 nm). The heading alignment condition, Eq. (10), is enforced within a range of $\Delta\psi_{\text{TAEM}} = 5$ deg. The bank-reversal threshold $\Delta\psi_{\text{threshold}}$ is designed to be a piecewise constant function of velocity. The solid lines in Fig. 1 show the heading-error variation and bank angle for the nominal case. The bank-reversal logic works well in commanding a total of three bank reversals. The final heading error is nearly zero. The solid lines in Fig. 2 depict the ground track (complete and zoom-in view) of the nominal trajectory. Clearly the ground track ends right on the circle centered at the HAC with radius

55.6 km, and the heading of the vehicle points directly at the HAC. Now, suppose that the actual lift coefficient of the vehicle is 90% of the modeled value, and the drag coefficient is 110% of the nominal value. Everything else remains unchanged, including the reference trajectory and bank reversal logic parameters. When the vehicle "reflies" the mission, the results are very different. The dashed line in the first subplot of Fig. 1 shows that the terminal heading error is in excess of 60 deg. The second subplot of Fig. 1 reveals the reason: the magnitude of the bank angle after the first bank reversal is about 20 deg smaller than that in the nominal case. Consequently, the vehicle does not have sufficient turning toward the HAC. Figure 2 gives the ground track of this case in dashed lines. The trajectory this time completely misses the TAEM circle by a distance of over 40 km. Given the sizes of the TAEM condition errors, it is unlikely that the vehicle would have had any chance of safe landing at the KSC. For comparison, the same aerodynamically dispersed case was also simulated with the new lateral guidance logic to be described in this paper. The longitudinal-tracking law was not changed. The simulation results are illustrated with the dotted line in Figs. 1 and 2. All of the TAEM conditions are met nearly perfectly, just as in the nominal case. The reasons for the success will be discussed later. It should be noted that no adjustments of the guidance law and lateral logic were made specifically for this case, and all of the guidance parameters in the proposed algorithms remain the same for all the simulation results presented in this paper.

B. Crossrange Parameter

The heading error with respect to the HAC plays the key role in the conventional bank-reversal criterion as given in Eq. (19). In this paper we consider a different but related parameter χ, defined to be

$$\chi = \sin^{-1}[\sin(s_{\text{togo}}) \sin \Delta\psi] \tag{20}$$

where the range-to-go s_{togo} and $\Delta\psi$ are the same as defined in Sec. II.B. In an Earth-centered Earth-fixed coordinate system, let $\boldsymbol{r}_{\text{HAC}}$ be the vector pointing from the origin to the HAC. Geometrically, χ is the angle between $\boldsymbol{r}_{\text{HAC}}$ and its projection on the plane formed by the current relative velocity and position vectors. Figure 3 shows the spherical triangle by which relationship (20) is derived. From Fig. 3 it is clear that χ represents the current dimensionless crossrange in radian. For the same reason as explained after Eq. (16), the value of χ in the subsequent discussion is cited in units of distance for the convenience of the reader. Obviously small heading error $\Delta\psi$ means small crossrange χ. Note that χ is still well defined and is zero at $s_{\text{togo}} = 0$, where $\Delta\psi$ has no definition. This property of χ can be convenient for vertical landing vehicles, where $s_{\text{TAEM}} \approx 0$ in the final range condition Eq. (9).

We have noticed that the crossrange parameter in general varies almost linearly with respect to the range between bank reversals. In contrast, the heading error always exhibits large and fast variation as the trajectory approaches the TAEM interface. Figure 4 shows the comparison of crossranges in km and heading errors for three different vehicles: the X-38 (a proposed crew-rescue vehicle for the International Space Station), X-33, and space shuttle. The hypersonic L/D values for these vehicles range from 0.7 to 1.2.

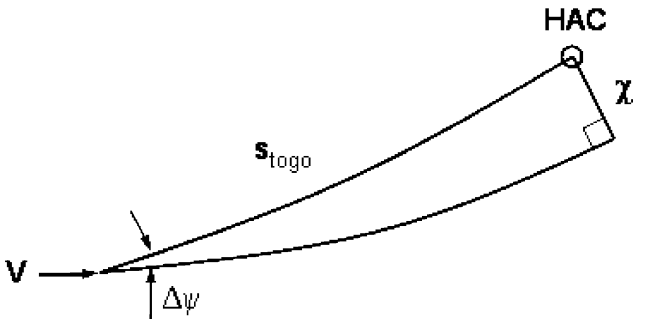

Fig. 3 Definition of the crossrange parameter χ.

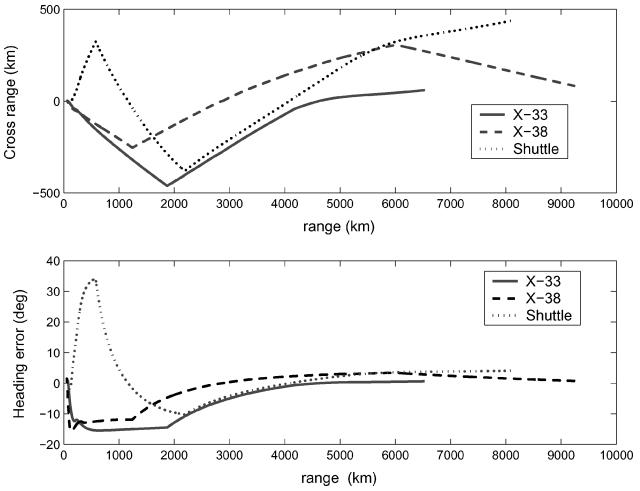

Fig. 4 Crossranges and heading errors for X-33, X-38, and shuttle.

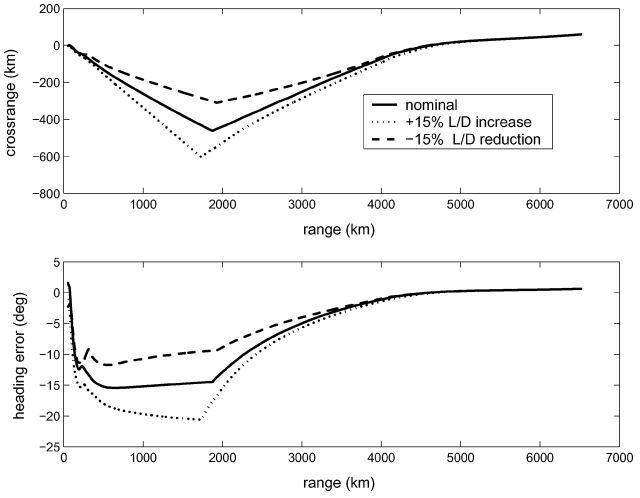

Fig. 5 Crossranges and heading errors of X-33 in nominal and changed *L/D* cases.

The trajectories are designed using the models of the vehicles in the algorithm by Shen and Lu,[2] subject to respective trajectory constraints and entry conditions for each individual vehicle. The X-33 and X-38 trajectories are planned with one bank reversal and the Shuttle with two reversals. The approximate piecewise linearity of the crossrange parameter, particularly in the second half of the trajectories, is evident for all the vehicles, whereas the heading error is more volatile and very different for different vehicles/missions. In Fig. 5 the crossranges and heading errors along three single bank-reversal trajectories for the X-33 are plotted. These three trajectories are generated with a nominal value of L/D for the X-33, higher L/D (increased by 15%), and lower L/D (reduced by 15%), respectively. In addition to the linearity of the crossranges, a proportional relationship between the crossranges and the perturbations in L/D holds quite well in the second half of the trajectory. The heading errors lack both characteristics.

The above observations suggest that the crossrange is a more suitable parameter with respect to which the bank-reversal conditions should be evaluated. A lateral guidance logic based on χ is likely to be less sensitive to the change of mission scenarios, and the effects of the design parameters on the final heading condition are probably more predictable. The linearity of the crossrange and its near proportionality make the scaling of the guidance parameters in such a lateral logic with respect to the variations in L/D more intuitive and simpler.

IV. Dynamically Adjusted Lateral Guidance Logic

The following discussion will assume that the reference trajectory has only one bank reversal, although the method is equally applicable to a reference trajectory with multiple bank reversals. For ensured TAEM heading precision, two bank reversals are planned in the guidance logic even though the reference trajectory has just one bank reversal. The lateral guidance logic has three sequential criteria that are designed for possible bank reversals in the first and second halves of the trajectory, respectively, plus a final correction near TAEM if necessary. Note that although the values of range to go are used in the following sections to separate the events and initiation of substeps in the guidance logic, the values of velocity or energy can easily be employed instead. Because the longitudinal-tracking law tracks the range-versus-energy profile tightly, the values of range and energy (velocity) have one-to-one correspondence.

We have found large aerodynamic dispersions of nearly constant percentages (not necessarily constant in magnitude) to be significantly more difficult for the entry guidance system to cope than rapidly varying dispersions. This is because the effects of these types of aerodynamic modeling uncertainties persist in the same direction throughout the entire trajectory, whereas the influence of fast-changing modeling uncertainties of similar size with zero mean tends to be averaged out to some extent. One of our emphases in this development is to handle large but slowly varying aerodynamic-modeling errors.

A. Preliminary

The lift-to-drag ratio plays an important role in the dynamic determination of the bank reversals. Define the ratio

$$\eta = (L/D)_{\text{est}}/(L/D)_{\text{ref}} \tag{21}$$

where $(L/D)_{\text{est}}$ is the estimated value for L/D based on the navigation data, and the subscript "ref" indicates the reference value hereafter. Given the Earth-relative velocity vector $\boldsymbol{V}$ and sensed total nongravity-acceleration vector $\boldsymbol{a}_{\text{Nav}}$, the drag acceleration during unpowered entry flight may be calculated by

$$D_{\text{Nav}} = -\boldsymbol{V}\cdot\boldsymbol{a}_{\text{Nav}}/V \tag{22}$$

Other forces such as those generated by the reaction control system are usually small and thus ignored. The lift acceleration is then computed from

$$L_{\text{Nav}} = \sqrt{a_{\text{Nav}}^2 - D_{\text{Nav}}^2} \tag{23}$$

To filter out possible spikes in the estimation of L/D due to noise, the computed values in Eqs. (22) and (23) are passed through a first-order low-pass filter:

$$(L/D)_{\text{est}}^k = e^{-\Delta t/\tau}(L/D)_{\text{est}}^{k-1} + (1-e^{-\Delta t/\tau})(L_{\text{Nav}}/D_{\text{Nav}}) \tag{24}$$

where k represents the current guidance cycle, $\tau > 0$ is the time constant of the filter, and $\Delta t > 0$ is the entry-guidance cycle time. The purpose of the estimation of the actual L/D in our guidance scheme is to detect long-term persistent aerodynamic-modeling errors. If short-duration spurs of considerable aerodynamic uncertainty in certain flight regimes are expected, a higher-order filter may be used to obtain an estimate of L/D averaged over a longer period.

The crossrange χ defined in Eq. (20) and its variation with respect to the range-to-go are at the center of our lateral guidance logic, the latter being given by

$$\chi' = \frac{\mathrm{d}\chi}{\mathrm{d}s_{\text{togo}}} = \frac{\cos s_{\text{togo}}\sin\Delta\psi + \Delta\psi'\sin s_{\text{togo}}\cos\Delta\psi}{\cos\chi} \tag{25}$$

where the prime means derivative with respect to s_{togo}, and

$$\Delta\psi' = -\frac{r}{V^2\cos\gamma\cos\Delta\psi}\left(\frac{L\sin\sigma}{\cos\gamma} + \frac{V^2}{r}\cos\gamma\sin\psi\tan\phi\right) - \psi'_{\text{LOS}} \tag{26}$$

The "line-of-sight" angle to the HAC is given by

$$\psi_{\text{LOS}} = \sin^{-1}\left[\frac{\sin(\theta_{\text{HAC}}-\theta)\cos\phi_{\text{HAC}}}{\sin s_{\text{togo}}}\right] \tag{27}$$

and when $s_{\text{togo}} \ll 1$ it is adequate to use the following simplified expression for the rate of ψ_{LOS}:

$$\psi'_{\text{LOS}} = \frac{\mathrm{d}\psi_{\text{LOS}}}{\mathrm{d}s_{\text{togo}}} = \frac{\tan\Delta\psi}{s_{\text{togo}}} \tag{28}$$

It is clear from Eq. (26) that the value of $\Delta\psi'$ changes if the sign of σ is changed. Using this observation in Eq. (25), we conclude that the value of χ' changes at any given point of the trajectory if the sign of σ is reversed.

B. Criterion for First Bank Reversal

For convenience the trajectory is divided into two halves by the point where the bank reversal along the reference trajectory takes place. Denote the range at this point by $s^R_{\text{togo}_{\text{ref}}}$. The exact time when the first bank reversal happens is not critical. The main function of the first bank reversal is to cause the second bank reversal to take place relatively close to the TAEM interface. Because of the inevitable presence of trajectory dispersions and disturbances, the lateral guidance logic will try to place the first bank reversal no later than the instant when the range reaches $s^R_{\text{togo}_{\text{ref}}}$. Otherwise there is a likelihood that the vehicle will not have sufficient time to turn around and align with the HAC, especially for missions with large initial crossranges. On the other hand, if the first bank reversal occurs too early, more bank reversals will subsequently occur than would otherwise be required. Many factors affect the "best" choice of when to perform the first bank reversal. Among them, we have identified that the actual value of L/D has the most pronounced influence. Obviously the smaller the actual L/D is, compared to its nominal value, the earlier the first bank reversal should be commanded relative to the reference bank reversal. The simplest approach is to choose a fixed bank reversal point defined by a specified sufficient amount of range bias earlier than $s^R_{\text{togo}_{\text{ref}}}$. But this approach may have to be very conservative if the vehicle is expected to fly missions with large crossranges, and substantial aerodynamic uncertainty is probable (that is, the first bank reversal must be commanded significantly earlier if mission-dependent tuning is to be avoided). We take an on-line approach here. Let $\Delta\psi^R_{\text{ref}}$ denote the heading error along the reference trajectory at the point of bank reversal (for a reference trajectory with multiple bank reversals, the last bank-reversal point is used). Define an "extended" reference crossrange χ_{ex} for $s_{\text{togo}} > s^R_{\text{togo}}$:

$$\chi_{\text{ex}} = \sin^{-1}\left(\sin s_{\text{togo}}\sin\Delta\psi^R_{\text{ref}}\right) \tag{29}$$

The geometric meaning of χ_{ex} is shown in Fig. 6 by the segment $\overline{RF}$, where the reference trajectory for a mission of the X-33 is used, and the reference crossrange variation is shown as a solid line. The point R in Fig. 6 is where the reference bank reversal occurs. The mirror image of the second half of the reference crossrange is also plotted as a dashed line in Fig. 6 and will be used later to determine the second bank reversal. The first bank reversal will take place when the condition

$$|\chi| \le c_1|\chi_{\text{ex}}|, \qquad \text{for} \qquad s_{\text{togo}} \ge s^R_{\text{togo}} \tag{30}$$

is violated. Thus χ_{ex} serves as a range-dependent threshold, resembling the criterion in Eq. (19). The coefficient c_1 is a scaling factor dependent on the estimated L/D and the level of aerodynamic uncertainty anticipated. Let $\bar{\eta}_{\max}$ be the expected maximum value of η in this phase as defined in Eq. (21), and $\bar{\eta}_{\min}$ the minimum value. These parameters reflect the confidence in the aerodynamic modeling of the vehicle and are given values. The maximum value of c_1 is set to 1, and its minimum value will be $c_{\min} > 0$. At any estimated value of η as given in Eq. (24), c_1 is calculated according to

$$c_1 = c_{\min} + \frac{\eta - \bar{\eta}_{\min}}{\bar{\eta}_{\max} - \bar{\eta}_{\min}}(1 - c_{\min}) \tag{31}$$

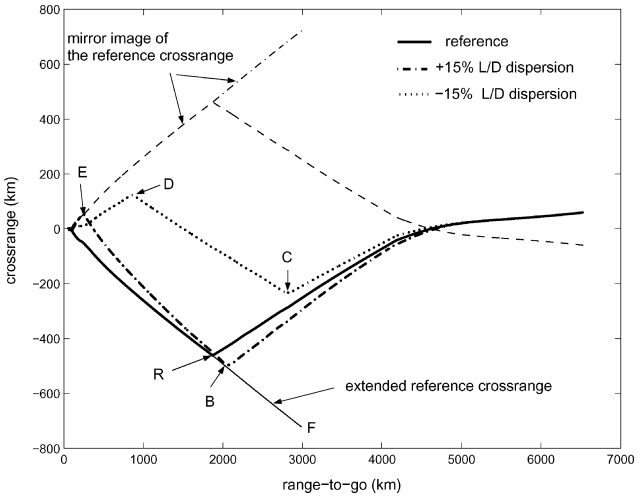

Fig. 6 Crossrange corridor used for bank-angle reversals.

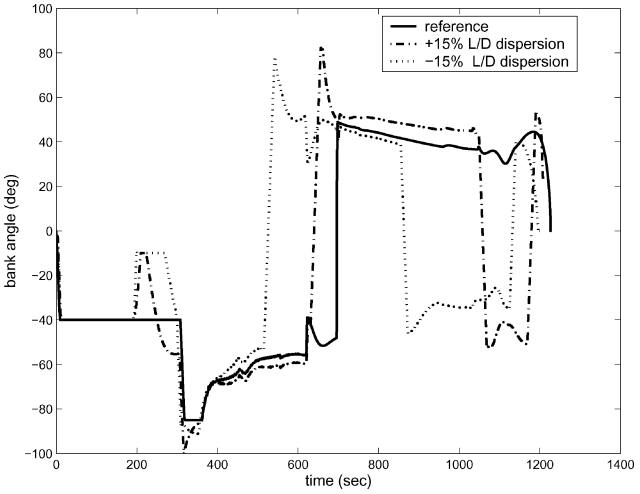

Fig. 7 Bank-angle histories for the three trajectories in Fig. 5.

The interpretation of this condition is that when the estimated actual L/D is lower than the nominal value, a small value of $c_1 \to c_{\min}$ will be used in the criterion (30) to force an earlier bank reversal. When the actual L/D is higher than the nominal, a larger value of c_1 (but no greater than 1) will be used. In this case the bank reversal will occur when the crossrange gets close to the extended crossrange χ_{ex}.

For the X-33, we set $\bar{\eta}_{\max} = 1.2, \bar{\eta}_{\min} = 0.8$. The value of $c_{\min} = 0.2$ works for all the cases reported in this paper. Figure 6 contains two cases with $\pm 15\%$ variations in L/D, respectively. This criterion found the first bank reversal for the case of weaker L/D at point C, significantly earlier than the reference bank reversal. For stronger L/D, the first bank reversal took place at point B, which is close to χ_{ex}. By design the first bank reversal in this case was still a little earlier than the reference bank reversal so a margin was left for the second half of the trajectory. Figure 7 shows the bank-angle histories for all three cases, including the reference. If the bank reversal for the case of 15% reduction in L/D occurs where the reference bank reversal happens, it will be too late to meet the final heading condition Eq. (10).

C. Criterion for Second Bank Reversal

In the second half of the trajectory the crossrange varies more linearly with respect to the range, as observed in Sec. III. After the range-to-go passes beyond the point s^R_{togo}, the second bank-reversal criterion is based on this approximate linearity and is aimed at satisfying the heading alignment condition Eq. (10). Recall from Eqs. (25) and (26) that the slope of χ changes when the sign of σ is reversed. We will use the notation $\chi'(-\sigma)$ to signify this changed

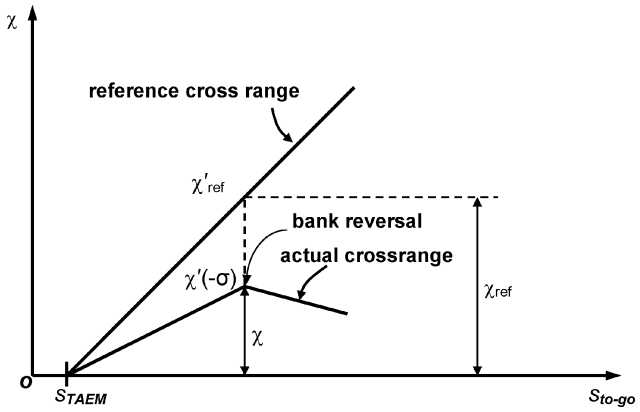

Fig. 8 Geometric illustration of the criterion for the second bank reversal.

slope of χ. Let χ_{ref} be the crossrange at the current range s_{togo}, and χ'_{ref} the slope of χ_{ref} at this point. When the current crossrange has sign opposite to that of the reference crossrange, χ_{ref} and χ'_{ref} will represent the value and slope of the mirror image of the reference crossrange.

If the crossrange-versus-range were truly a straight line, the point where the second bank reversal should occur is illustrated in Fig. 8. At this point if the sign of σ is reversed, the current crossrange χ and the changed slope $\chi'(-\sigma)$ should satisfy the relationship

$$|\chi| = |[\chi'(-\sigma)/\chi'_{\text{ref}}]\chi_{\text{ref}}| \tag{32}$$

This condition corresponds to the requirement that the combination of χ and its slope $\chi'(-\sigma)$ results in zero crossrange at the TAEM range s_{TAEM}, as it is along the reference trajectory, which is equivalent to $\Delta\psi_f = 0$. Because the crossrange is not exactly linear, and dispersions after the bank reversal could cause the actual trajectory to fall short in the direction it needs to turn, the right-hand side of Eq. (32) is multiplied by a coefficient $0 < c_2 < 1$ to add a margin. Hence the second bank reversal takes place when the following condition is violated:

$$|\chi| \le c_2|[\chi'(-\sigma)/\chi'_{\text{ref}}]\chi_{\text{ref}}| \tag{33}$$

The smaller c_2 is, the more conservative this criterion is. A more conservative criterion ensures that the bank reversal is not too late for all the cases but could, in some cases, command the bank reversal too early so that additional reversals would be needed later. The selection of c_2 should strike a balance. For the X-33 and the sizes of aerodynamic uncertainties present in the simulations reported in this paper (Sec. VI), and when used in conjunction with the final bank-reversal predictor in Sec. IV.D, a constant value of $c_2 = 0.7$ was found to be appropriate.

When the navigation-derived aerodynamic lift acceleration L_{Nav}, much like what is described in Eqs. (23) and (24), is deemed reliable, it can be used in the calculation of $\chi'(-\sigma)$ in Eq. (33) to account for the effects of the difference between the nominal and actual values of L.

If the reference crossrange were truly linear with respect to s_{togo}, it would be evident from Fig. 8 that $\chi_{\text{ref}}/\chi'_{\text{ref}} = s_{\text{togo}} - s_{\text{TAEM}}$. So the criterion (33) could take the alternate form of

$$|\chi| \le c_2|\chi'(-\sigma)|(s_{\text{togo}} - s_{\text{TAEM}}) \tag{34}$$

This version of the second criterion does not require the data on the reference crossrange profile. It tends to be more conservative than Eq. (33) for the same value of c_2. Therefore a larger c_2 may be used in relation (34).

In some dispersed cases for a mission with large crossrange, the first criterion in Eq. (30) may never become active in the first part of the trajectory defined by $s_{\text{togo}} \ge s^R_{\text{togo}}$. The second criterion in Eq. (33) will still take effect after $s_{\text{togo}} < s^R_{\text{togo}}$, regardless of whether the criterion in Eq. (30) was activated.

In Fig. 6, the second bank reversal points found by criterion Eq. (33) are at locations E and D for the trajectories of the X-33 with $\pm 15\%$ dispersions in L/D. Notice that the crossranges are very different for the two cases for the same vehicle and the same mission (one flew just about half of the maximum crossrange the other had).

D. Pre-TAEM Bank-Reversal Prediction

After the bank reversal(s) determined by criteria in Eqs. (30) and (33), a final correction on the heading may be needed near the TAEM interface because the previous bank reversal may have overcorrected the heading, and the vehicle is continuously subject to winds and the same sources of dispersion. This last bank reversal should be performed only when necessary, and the final heading precision yielded by the last bank reversal must be within specification. Toward these goals, a numerical predictor method is used once the velocity of the vehicle is below a preset value $V_{\text{pre-TAEM}} > V_{\text{TAEM}}$ (alternatively, a preset value of range-to-go may be used instead). The prediction on whether a last bank reversal will be needed is made as follows: Starting from the current condition given from the navigation data, the equations of motion, Eqs. (1–6) are numerically integrated with the TAEM interface, with $|\sigma|$ and α provided by exactly the same longitudinal-tracking laws used for guidance. But the sign of σ opposite to the current bank-angle sign is used in the integration. This numerical integration is carried out only once in every guidance cycle and no iterations will be involved. The sign of the actual guidance command for σ remains the same in the current guidance cycle as determined by the criterion Eq. (33), if the predicted final heading error $\Delta\psi_f$ does not change to the opposite of the polarity of $\Delta\psi_f$ in the last cycle. Thus the numerical integration is predicting "what will happen to the final heading error if a bank reversal is taken now." When the predicted $\Delta\psi_f$ does change sign, it indicates that a final bank reversal performed now would null the final heading error. A bank reversal is commanded at this point. If the bank angle sign remained unchanged in such a case, the TAEM heading error would likely exceed the tolerance set in Eq. (10). It should be stressed again that this numerical prediction is designed only for the cases in which the previous bank reversal overcorrects the trajectory. If this final compensation is desired to be used, it may be advisable to set the parameter c_2 a little more conservatively in the criterion in relation (33) or (34) so that undercorrections do not occur in all dispersed cases.

Because the duration of the remaining flight is already relatively short in this phase, and no repeated integrations are needed in each guidance cycle, the numerical integrations should not pose great difficulty for the guidance computer. The short duration also contributes to the good precision of the prediction. The rate and acceleration limits on the bank angle can be incorporated into the integrations so that the effects of these limits on the bank reversal and trajectory can be taken into account in the prediction.

For all of the simulations shown in this paper, the numerical prediction started at $V_{\text{pre-TAEM}} = V_{\text{TAEM}} + 550$ m/s. As can be seen from Figs. 6 and 7, in both cases of $\pm 15\%$ dispersions in L/D, the numerical bank-reversal prediction resulted in a final correction, and the final heading errors were nearly zero. In both cases the TAEM range errors were less than 1 km.

The preceding numerical bank-reversal predictor is optional and is intended for the cases where high final heading-alignment precision is important. The numerical predictor may be effectively turned off by setting the activation velocity $V_{\text{pre-TAEM}} = V_{\text{TAEM}}$, if very high TAEM heading precision is not required. In such a case, the criterion (33) will be responsible for determining the second bank reversal, and the third if necessary. In these cases it is advisable to gradually tighten the coefficient c_2 in Eq. (33) as the vehicle approaches the TAEM interface. A possible selection is

$$c_2 = c_{2_{\max}} + \left(\frac{V - V_{\text{ref}}^R}{V_{\text{TAEM}} - V_{\text{ref}}^R}\right)\left(c_{2_{\min}} - c_{2_{\max}}\right) \tag{35}$$

where V_{ref}^R is the velocity at the bank-reversal point along the reference trajectory (or at the last bank-reversal point if multiple bank reversals are present along the reference trajectory), $0 < c_{2_{\max}} < 1.0$ is the maximum value for c_2, and $0 < c_{2_{\min}} (< c_{2_{\max}}) < 1.0$ is the minimum value for c_2. For the X-33, $c_{2_{\max}} = 0.9$ and $c_{2_{\min}} = 0.4$ appear to be appropriate choices that will meet the TAEM heading requirement without causing excessive bank reversals.

The lateral guidance logic developed in this paper is summarized in the following sequential steps as the entry flight progresses:

1) Before the range-to-go reaches the point where the reference bank reversal takes place ($s_{\text{togo}} \geq s_{\text{togo}}^R$), the criterion in Eq. (30) determines the bank reversal.

2) When $s_{\text{togo}} < s_{\text{togo}}^R$, but $V \geq V_{\text{pre-TAEM}}$, the criterion in Eq. (33) [or Eq. (34)] is responsible for bank reversal. If criterion (33) is to be used throughout the remaining part of the entry flight, the coefficient c_2 should be gradually tightened, as in Eq. (35).

3) If high precision in TAEM heading alignment is required, the optional numerical bank-reversal predictor takes over to determine whether a last bank reversal is needed to null the final heading error when $V_{\text{TAEM}} \leq V \leq V_{\text{pre-TAEM}}$ as the vehicle is moving closer to the TAEM interface.

V. Longitudinal Tracking Laws

Although not stated explicitly, the working assumption for the lateral guidance logic above is that the reference longitudinal profile (range versus energy) is being tracked closely by the longitudinal guidance law. This precision is important for the lateral guidance logic to function correctly. It has been reported that for longitudinal tracking, a linear proportional controller with time-varying gains generated using the linear–quadratic regulator (LQR) method works remarkably well. One set of LQR gains is sufficient for a given vehicle, even if the vehicle may need to fly very different missions/trajectories.[7] We have found that adding an integral term to the control law can enhance the performance noticeably, particularly in the presence of significant aerodynamic modeling mismatch. For instance, for a case of 20% reduction in the actual L/D for the X-33 as shown in Figs. 1 and 2, the TAEM range error is just 0.5 km with the integral term in the control law, whereas the range error is over 10 km without the integral term. When modulations of both σ and α are available for guidance, the proportional-plus-integral (PI) tracking law takes the form of

$$\boldsymbol{u}_e = \begin{pmatrix} \delta\sigma_e \\ \delta\alpha_e \end{pmatrix} = -\boldsymbol{K}_p(e)\delta\boldsymbol{x}_{\text{lon}} - \boldsymbol{k}_I(e)\int \delta s_{\text{togo}}\,\mathrm{d}e \tag{36}$$

where $\delta\boldsymbol{x}_{\text{lon}} = (\delta s_{\text{togo}}, \delta r, \delta\gamma)^T$ is the dispersion vector in the longitudinal state and $\boldsymbol{K}_P \in R^{2\times 3}$ and $\boldsymbol{k}_I \in R^2$ are the feedback gains scheduled with respect to the energy e. Rigorous theory is available on the robustness properties of multi-input systems with this type of controllers,[9] and tailored applications in aerospace control have demonstrated the effectiveness of these controllers.[10] The actual bank angle command will have a magnitude of

$$|\sigma| = |\sigma_{\text{ref}}| + \delta\sigma_e \tag{37}$$

where $\delta\sigma_e$ is capped so that $|\sigma_{\text{ref}}| + \delta\sigma_e \geq 0$. The sign of σ is determined by the lateral logic discussed in Sec. IV. The gains at a fixed e in the control law can be found by the LQR approach based on the linearized longitudinal dynamics at that e. Rules of thumb for designing LQR gains to track the longitudinal profile described by Dukeman[7] may still be used as guidelines.

When the modulation of α is available for entry guidance, we have found that the following simple constant-gain guidance law helps provide remarkably tight range control:

$$\delta\alpha_c = -k_\alpha \delta s_{\text{togo}} - k_{\alpha I}\int \delta s_{\text{togo}}\,\mathrm{d}e \tag{38}$$

The constant gains k_α and $k_{\alpha I}$ are selected in a straightforward fashion: suppose that for 1-km dispersion in range, an excursion of 1 deg in α is allowed. Then $k_\alpha = 1$ deg/km. Because the dimensionless energy e varies from about 0.5 to nearly 1.0 along the entry trajectory, $k_{\alpha I} = 2$ deg/km corresponds to 1 deg of α increment for the integration of an average of 1-km range error. The negative signs in

Eq. (38) simply reflect the fact that a lower angle of attack should be used when the actual range-to-go is longer than the reference value (i.e., $\delta s_{\text{togo}} = s_{\text{togo}} - s_{\text{togo}_{\text{ref}}} > 0$). It should not be a surprise that the control of α regulates the range well, because the variations of α directly affect the drag D, which in turn changes the rate of s_{togo} through Eq. (25). The clear physical meaning of the tracking law (38) helps explain why it is so effective in the second half of the trajectory, where the aerodynamic controls have a stronger influence in shaping the trajectory. On the other hand, this simple guidance law can be too demanding in the early part of the entry flight where the dynamic pressure is low, causing unnecessary control saturations and stability issues. Therefore a logical approach is to blend $\delta\alpha_e$ in Eq. (36) and $\delta\alpha_c$ in Eq. (38) together. The combined α guidance law for longitudinal tracking is then

$$\delta\alpha = w(V)\delta\alpha_e + [1 - w(V)]\delta\alpha_c \tag{39}$$

where $0 \le w(V) \le 1$ is taken to be a velocity-dependent weighting that is given by

$$w(V) = \begin{cases} 1.0, & V > V_{\text{blend}} \\ (V - V_{\text{TAEM}})/(V_{\text{blend}} - V_{\text{TAEM}}), & V_{\text{TAEM}} \le V \le V_{\text{blend}} \end{cases} \tag{40}$$

The value of V_{blend} is chosen to be (somewhat arbitrarily) in the range of 5000–7000 m/s. The control law (39) therefore gives a $\delta\alpha$ that starts with $\delta\alpha_e$ and gradually switches to $\delta\alpha_c$ as the TAEM interface is approached.

Although the bank angle is still the chief trajectory control, the blended control law (39) is found to contribute to very consistent and impressive range precision at the TAEM interface. No excessive α modulations were commanded beyond what the LQR-based PI control law (36) would call for. Another benefit is that the blending in Eq. (39) appears to considerably reduce the necessity for high-quality gains $\boldsymbol{K}_p$ and $\boldsymbol{k}_I$ as in the case when only the PI control law (36) is used. In fact, we have used the same gains $\boldsymbol{K}_p$ and $\boldsymbol{k}_I$ for several vehicles with very different sizes, weights, and aerodynamics (including those in Fig. 4). The performance is similar in all the cases. Because the range-versus-energy profile provides the primary parameters that determine the longitudinal motion of the entry flight, the burden of tuning the gains $\boldsymbol{K}_p$ and $\boldsymbol{k}_I$ is much alleviated with the simple blended-control law (39), and the performance of the longitudinal tracking is still ensured.

VI. Validation by Extensive Simulations

The simulation environment is a high-fidelity simulation tool developed at the NASA Marshall Space Flight Center, dubbed Marshall Aerospace Vehicle Representation In C (MAVERIC). The models of the subsystems of the X-33 are available in MAVERIC. The mission scenarios are based on the nine orbital-entry missions first described in Ref. 11. All of the missions are for horizontal landing at the KSC. Table 1 lists the entry conditions of the nine missions. These missions are divided into three groups, separated by the steepness of the entry flight path angles and the inclinations of the orbits from which the X-33 returns to the Earth. The first mission in each group (AGC13, 16, and 19) represents entry flight from the ideal deorbit opportunity. The initial crossranges are small in these cases. The next two missions in each group are for the cases when the deorbit maneuver takes place one orbit earlier and one orbit later than the best opportunity, respectively. The consequence is a large right crossrange or a large left crossrange at the entry interface. These large crossranges are close to the maximum crossrange capability of the X-33 in these cases. The negative crossranges in Table 1 indicate left crossranges.

To demonstrate the autonomous capability of the entry guidance system based on the guidance method presented in this paper and the trajectory-planning algorithm in Ref. 2, all of the guidance parameters were kept the same for all the simulations shown in this paper, and no mission-dependent or case-dependent tuning was done. Owing to the lack of a control system module for the X-33 applicable in orbital-entry-flight regimes, simulations were performed in 3DOF mode.

Table 1 Entry conditions at the altitude of 121.92 km (400,000 ft)

Mission	Inclination, deg	V_0, m/s	Range, km	Crossrange, km	γ_0, deg
AGC13	51.6	7622.0	6519	59	−1.4379
AGC14	51.6	7621.30	6554	809	−1.4380
AGC15	51.6	7622.79	6589	−848	−1.4376
AGC16	51.6	7625.0	8160	148	−1.2492
AGC17	51.6	7625.15	8715	883	−1.2493
AGC18	51.6	7625.72	8197	−778	−1.2490
AGC19	28.5	7442.37	7365	274	−1.0275
AGC20	28.5	7442.07	7389	759	−1.0275
AGC21	28.5	7440.12	7626	482	−1.0278

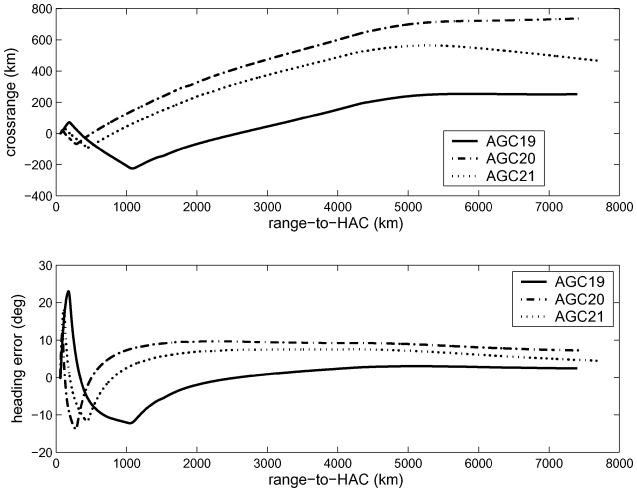

Fig. 9 Crossranges and heading errors along the nominal trajectories for missions AGC19–21.

A. Nominal Cases

The nominal case simulations provide a quick verification of the principles of the entry guidance design and an assessment of how well the algorithms work in different mission scenarios. Throughout the rest of Sec. VI, a 3DOF reference trajectory is generated on-line[2] at the beginning of each simulation. All of the trajectory-path constraints, TAEM constraints, and control-authority constraints specified in Ref. 11 are imposed in the trajectory planning. The entry guidance algorithms described in Secs. IV and V produce the guidance commands in bank angle and angle of attack hereafter in each guidance cycle at the rate of 1 Hz. Monthly average winds are used in the simulations based on the Global Reference Atmospheric Model (GRAM).[12] The simulation stops when the velocity has reached the prespecified TAEM value.

All nine nominal missions were flown successfully with high precision on the imposed conditions. In particular, the TAEM conditions were met with range errors less than 1.85 km (1 nm) and heading errors less than 1 deg in all cases. Figures 9–11 show the results for the three missions of AGC19–21. Figure 9 depicts the crossrange and heading errors. Returning from a minimum-inclination orbit achievable from the KSC, all three missions have positive crossranges at entry interface. (In fact, mission AGC21 enters the atmosphere at a latitude of 22.8° north, not much lower than the 28.5° latitude of the KSC.) The crossranges still exhibit good linearity in the later part of the trajectories, whereas the heading errors become more erratic toward the end. The histories of bank angle and angle of attack are plotted in Fig. 10. Two bank reversals were used to null the TAEM heading errors. It can be seen that the first bank reversals for both AGC20 and 21 occurred quite late, an indication that the vehicle was nearly at its crossrange capability limit in those two cases. The altitude-versus-velocity and range-versus-specific-energy variations are shown in Fig. 11, where the specific energy

Table 2 Statistics on TAEM conditions (100 dispersed runs for each mission)

Case	Parameter	Target value	Mean	Max	Min	Std. deviation
AGC13	$\Delta\psi_f$, deg	Within ±5 deg	−0.37	0.91	−1.61	0.48
	Range-to-HAC, km	55.6	56.025	58.773	53.505	1.330
	Altitude, km	30.427	30.268	30.674	29.838	0.204
AGC14	$\Delta\psi_f$, deg	Within ±5 deg	0.81	4.4	−1.01	0.81
	Range-to-HAC, km	55.6	54.674	56.898	52.777	1.036
	Altitude, km	30.427	29.912	30.806	29.347	0.303
AGC15	$\Delta\psi_f$, deg	Within ±5 deg	0.18	1.95	−0.72	0.41
	Range-to-HAC, km	55.6	54.943	58.155	52.012	1.338
	Altitude, km	30.427	30.267	30.997	29.676	0.284
AGC16	$\Delta\psi_f$, deg	Within ±5 deg	1.15	4.04	−1.11	0.99
	Range-to-HAC, km	55.6	55.920	58.636	52.570	1.343
	Altitude, km	29.431	29.787	30.321	29.363	0.211
AGC17	$\Delta\psi_f$, deg	Within ±5 deg	−0.38	5.25	−3.67	1.14
	Range-to-HAC, km	55.6	54.348	57.756	52.043	1.284
	Altitude, km	29.431	29.569	30.592	28.396	0.522
AGC18	$\Delta\psi_f$, deg	Within ±5 deg	0.35	5.11	−1.91	1.20
	Range-to-HAC, km	55.6	54.782	57.934	52.085	1.310
	Altitude, km	29.431	29.453	30.214	28.462	0.383
AGC19	$\Delta\psi_f$, deg	Within ±5 deg	−0.49	1.42	−2.67	0.78
	Range-to-HAC, km	55.6	56.264	59.327	52.959	1.573
	Altitude, km	29.431	29.526	30.146	29.049	0.227
AGC20	$\Delta\psi_f$, deg	Within ±5 deg	−0.82	1.30	−2.96	0.90
	Range-to-HAC, km	55.6	54.282	57.554	51.991	1.381
	Altitude, km	29.431	29.702	30.720	28.276	0.591
AGC21	$\Delta\psi_f$, deg	Within ±5 deg	−0.22	1.63	−3.57	0.83
	Range-to-HAC, km	55.6	53.729	56.229	51.041	1.594
	Altitude, km	29.431	29.842	30.684	28.677	0.416

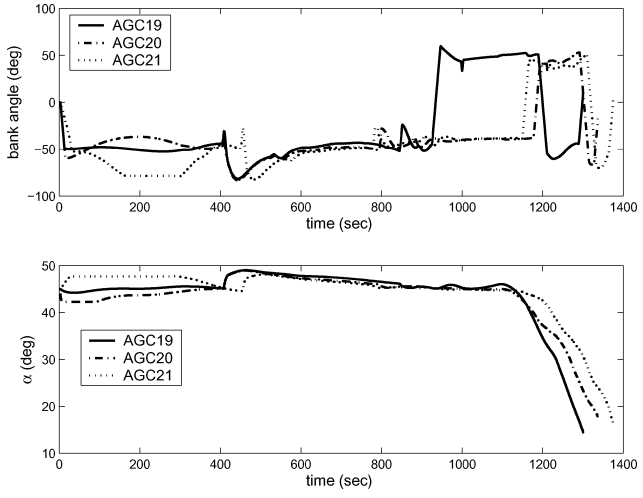

Fig. 10 Nominal bank angle and α profiles for missions AGC19–21.

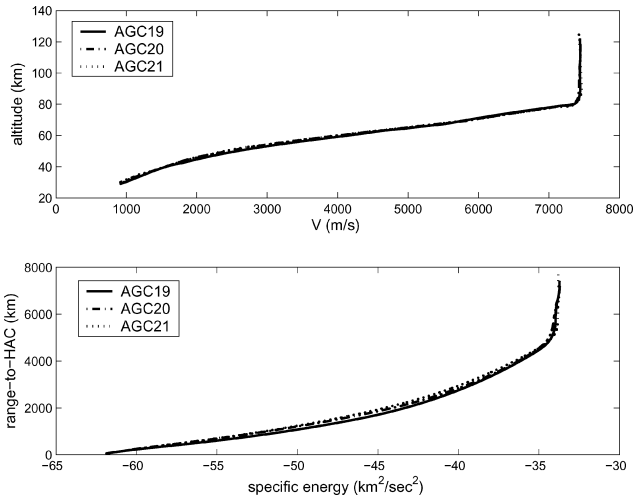

Fig. 11 Nominal longitudinal profiles for missions AGC19–21.

used is the dimensional version of $-e$, with e given in Eq. (17). Notice that the trajectories in the velocity–altitude space are very close. The differences in the range–energy profiles are more visible but still seem relatively minor. Yet the differences in the bank angle profiles seen in Fig. 10 are significant. Finally, Fig. 12 contains the heat-rate variations along the three trajectories. The imposed constraints on peak heat rate for the three missions is 680.935 kW/m^2 (60 BTU/ft^2-s). This is a remarkably stringent constraint, but the trajectory-planning and guidance algorithms enforce it accurately in all three cases.

B. Dispersion Testing

The built-in capability of MAVERIC allows dispersion simulations with respect to uncertainties in aerodynamics, navigation data, and vehicle mass. Random atmospheric dispersions and winds are generated from the GRAM. The 1σ uncertainties in the lift and drag coefficients are given in tabular form as functions of Mach number and angle of attack,[13] and the 3σ values represent about 10% uncertainty in C_L and 6% in C_D during the entry phase. While C_L and C_D are dispersed independently in each simulation within their respective 3σ uncertainties, the maximum dispersion in the ratio of C_L/C_D is capped (in both plus and minus directions) by a Mach-dependent limit. This limit in hypersonic regions amounts to about an average of ±6% variations in L/D at $\alpha = 45$ deg. If the dispersions ΔC_L and/or ΔC_D result in a variation of C_L/C_D exceeding the limit, ΔC_L and ΔC_D are adjusted so that the limit is maintained.

Table 2 summarizes the statistics on the TAEM conditions. For each of the nine missions, a total of 100 dispersed trajectories were run. For each parameter (heading error, range, and altitude), the target value, the mean for the 100 runs, the maximum and minimum values among the 100 runs, and the standard deviation are given in the table. A final heading error within ±5 deg is considered perfect. The small values for the means and standard deviations for $\Delta\psi_f$ in all nine missions indicate that the heading errors are all well within

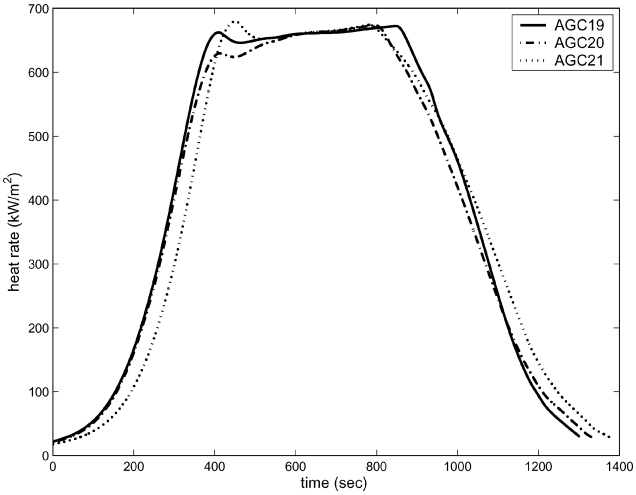

Fig. 12 Heat-rate variations along the nominal trajectories for missions AGC19–21.

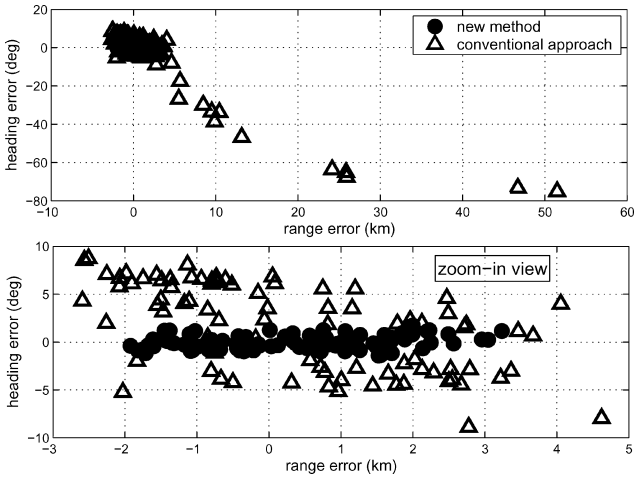

Fig. 13 Comparison of TAEM condition errors for mission AGC13 with increased aerodynamic uncertainty (100 runs).

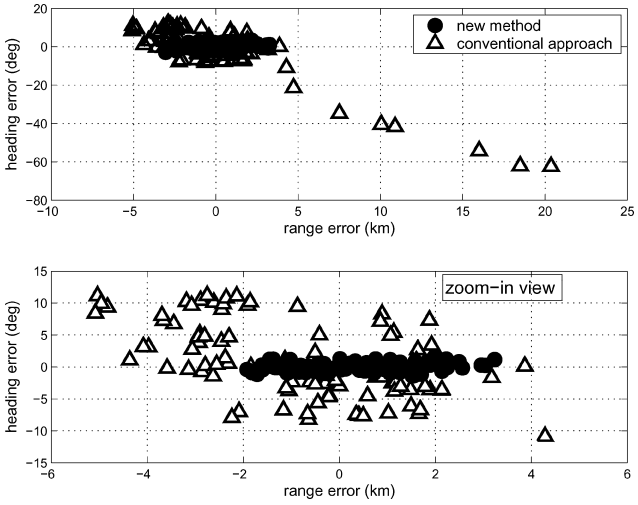

Fig. 14 Comparison of TAEM condition errors for mission AGC16 with increased aerodynamic uncertainty (100 runs).

this range, except for two runs where $\Delta\psi_f$ are slightly over 5 deg. The largest TAEM range error is about 4.5 km (less than 2.5 nm), and in most cases the range error is within 2 km. The TAEM altitudes also have means very close to the target values and the standard deviations are small. The precision seen in Table 2 represents a considerable improvement as compared to the tracking results in Ref. 2.

C. Large Random and Multiplicative Aerodynamic Dispersions

The ability of this guidance algorithm to accommodate significant aerodynamic modeling mismatches is further tested with increased dispersions in C_L and C_D. Both large random dispersions and large dispersions of constant percentages are used. In the first category, the MAVERIC dispersion setup is modified so that the 3σ aerodynamic uncertainty is doubled. The uncertainty is still a function of Mach number and α, but the size is doubled for the same random seed. The allowable limit on the variations of L/D is increased to $\pm 15\%$ instead of $\pm 6\%$ in the preceding section. The sizes of other dispersions in navigation data, mass, atmosphere, and winds remain the same. Only missions AGC13, 16, and 19 are tested, because with the dramatically increased aerodynamic dispersions, there will be cases in the other missions where the vehicle cannot land at the KSC due to the large initial crossranges.

For comparison with the conventional approach, a velocity-dependent $\Delta\psi_{\text{threshold}}(V)$ is carefully designed for the conventional bank-reversal logic, Eq. (19). When combined with a proportional LQR tracking law described in Ref. 7 for longitudinal tracking, this guidance approach gives the same level of performance as seen in Table 2 for the same dispersions in Sec. VI.B in missions AGC13, 16, and 19. This same guidance algorithm is also applied here when the aerodynamic uncertainty is increased.

Again a total of 100 runs are made for each of the three missions. The performance of the new method for all three mission is statistically the same as the results in Table 2. The conventional approach, however, renders different performances for different missions. Figures 13–15 show the comparison of the two methods in terms of the heading errors and range errors at the TAEM interface for the three missions. The scatter of the TAEM conditions under the new guidance method is consistently tight in all three missions and the errors are small without exception. In comparison, the conventional approach misses the TAEM range and heading conditions very badly in 12% and 8% of the cases, respectively, in missions AGC13 and 16. According to the scoring criteria in Ref. 6, the conventional approach would have been judged to have failed the mission AGC13. Even when these worst cases are removed, the zoom-in views in Figs. 13 and 14 reveal that the new method still outperforms the conventional approach by a good margin. In mission AGC19, the conventional approach performs better than it does in the other two missions in that the worst cases are less severe. But the superiority of the new method is no less evident even in this mission, as seen in Fig. 15.

The second testing category in this section is created to assess how the guidance method handles large and persistent aerodynamic modeling errors. To this end, the values of C_L and C_D used in the simulations are perturbed by constant percentages up to $\pm 20\%$ relative to their nominal values C_L^* and C_D^*. The dispersions are unknown to both the trajectory planning algorithm and guidance algorithm. The original 3σ data in Ref. 12 for the uncertainty in C_L and C_D of the X-33 are constant (but at smaller magnitude) for Mach > 10. The values of C_L and C_D are also nearly constant in that region because the angle of attack is almost constant (cf. Fig. 10), and the aerodynamic coefficients are essentially independent of the Mach number in hypersonic region. Hence constant percentage dispersions in C_L and C_D would be reasonable assumptions in hypersonic region when α remains nearly constant. The same multiplicative dispersions in C_L and C_D would probably be less representative when the vehicle is close to the TAEM interface and α begins to decrease. But when the dispersions used in the testing are sufficiently large, one can view this setting as a "worst-case" scenario of aerodynamic uncertainty in which the guidance algorithms are evaluated (recall that large and nonmultiplicative aerodynamic dispersions have already been used above, and the good performance of the present guidance algorithm has been shown (Table 2 and Figs. 13–15).

In the presence of large constant-percentage dispersions in C_L and C_D, the new guidance algorithm and the proportional LQR tracking law with conventional bank-reversal logic are applied to

Table 3 Comparison of TAEM condition errors under the new and conventional guidance approaches with constant percentage aerodynamic dispersions (mission AGC19)

Method	$\Delta\psi_f$, deg	ΔRange, km	ΔAltitude, km
Case 1: $\Delta C_L/C_L^* = -10\%$, $\Delta C_D/C_D^* = +10\%$			
New	−0.076	−0.967	−0.844
Conventional	3.35	3.941	0.412
Case 2: $\Delta C_L/C_L^* = +10\%$, $\Delta C_D/C_D^* = -10\%$			
New	−2.01	−0.348	2.186
Conventional	−8.197	−10.525	−0.640
Case 3: $\Delta C_L/C_L^* = +20\%$, $\Delta C_D/C_D^* = 0\%$			
New	−0.083	−1.548	0.608
Conventional	−5.81	−7.412	0.159
Case 4: $\Delta C_L/C_L^* = 0\%$, $\Delta C_D/C_D^* = +20\%$			
New	−1.186	−1.856	−0.469
Conventional	3.083	5.770	0.911
Case 5: $\Delta C_L/C_L^* = +20\%$, $\Delta C_D/C_D^* = +20\%$			
New	1.329	−0.806	0.399
Conventional	7.290	2.580	1.020
Case 6: $\Delta C_L/C_L^* = -20\%$, $\Delta C_D/C_D^* = -20\%$			
New	−2.276	0.964	−0.164
Conventional	−2.016	−2.628	−1.081
Case 7: $\Delta C_L/C_L^* = -20\%$, $\Delta C_D/C_D^* = +20\%$			
New	−5.512	−2.020	−1.797
Conventional	−3.873	100.601	0.221

Note: Dispersions are given following case numbers.

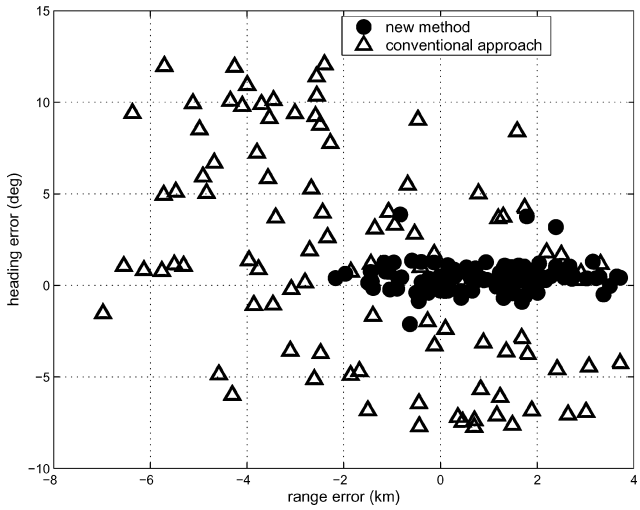

Fig. 15 Comparison of TAEM condition errors for mission AGC19 with increased aerodynamic uncertainty (100 runs).

guide the vehicle. Mission AGC19 is chosen because this is the mission where the conventional approach is seen to work the best in the presence of larger random aerodynamic uncertainties. The reference trajectory is generated based on the nominal aerodynamic model. The constant-percentage dispersions are applied to C_L and C_D in MAVERIC simulations. The limit on the maximum dispersion of L/D is removed. Table 3 lists a comparison of the TAEM condition errors in several test cases. The conventional approach actually turns in acceptable performances in four out of the seven cases, a testament to the strengths of the conventional method (although the conventional approach would fail in most of those cases in missions AGC13 and 16). The new method, however, continues to outperform the conventional method in every case by providing considerably smaller TAEM condition errors. Even in the most difficult situation of the last case where C_L is reduced by 20% and C_D increased simultaneously by 20%, the new method still produces a TAEM heading error of just −5.5 deg and a range error of only 2 km, in sharp contrast to the 100-km range error under the conventional approach. The altitude error is somewhat large in this case, but is likely still within the recoverable margin for a safe landing. The success under this extreme situation highlights the capability and robustness of the entry guidance method presented in this paper.

VII. Conclusions

The goal of this work is to develop a lateral entry guidance approach that has the following traits: 1) reliability and good performance, 2) robustness with respect to significant aerodynamic uncertainty, and 3) systematic design procedure and no need for mission- or case-dependent tuning. The lateral guidance logic presented in this paper accomplishes the goals by determining bank reversals according to two dynamically adjusted criteria and a bank-reversal predictor using numerical trajectory propagation. The finding that the crossrange is nearly linear with respect to the range and much better behaved than the heading error sets the foundation of the bank-reversal criteria. To account for the great influence of large aerodynamic uncertainty, the criteria allow the estimated lift-to-drag ratio derived from navigation data to be incorporated. The validation of the guidance algorithm is done through extensive testing in a high-fidelity simulation environment involving a wide range of missions and significant dispersions. The results of the tests conducted in this study show that this method outperforms the conventional approach, with significant margins in stressful cases.

The full potential of the present entry guidance method would be best utilized when the method is combined with an on-board trajectory-planning algorithm to provide complete autonomy for the entry guidance system (as is done in the simulations in this paper). The method, however, is equally applicable when the reference trajectory is preloaded.

References

[1]Harpold, J. C., and Graves, C. A., "Shuttle Entry Guidance," *Journal of the Astronautical Sciences*, Vol. 37, No. 3, 1979, pp. 239–268.

[2]Shen, Z., and Lu, P., "On-Board Generation of Three-Dimensional Constrained Entry Trajectories," *Journal of Guidance, Control, and Dynamics*, Vol. 26, No. 1, 2003, pp. 111–121.

[3]Mease, K. D., Chen, D. T., Teufel, P., and Schoenenberger, H., "Reduced-Order Entry Trajectory Planning for Acceleration Guidance," *Journal of Guidance, Control, and Dynamics*, Vol. 25, No. 2, 2002, pp. 257–266.

[4]Zimmerman, C., Dukeman, G., and Hanson, J., "An Automated Method to Compute Orbital Entry Re-Entry Trajectories with Heating Constraints," *Journal of Guidance, Control, and Dynamics*, Vol. 26, No. 4, 2003, pp. 523–529.

[5]Lu, P., "Regulation About Time-Varying Trajectories: Precision Entry Guidance Illustrated," *Journal of Guidance, Control, and Dynamics*, Vol. 22, No. 6, 1999, pp. 784–790.

[6]Hanson, J.,"Integration and Testing of Advanced Guidance and Control (AG&C) Technologies (ITAGCT)," Advanced Guidance and Control Workshop, NASA Marshall Space Flight Center, July 2003.

[7]Dukeman, G. A.,"Profile-Following Entry Guidance Using Linear Quadratic Regulator Theory," AIAA Paper 2002-4457, Aug. 2002.

[8]Saraf, A., Leavitt, J. A., Chen, D. T., and Mease, K. D., "Design and Evaluation of an Acceleration Guidance Algorithm for Entry," AIAA Paper 2003-5737, Aug. 2003.

[9]Desoer, C. A., and Wang, Y. T., "Linear Time-Invariant Robust Servomechanism Problem: A Self-Contained Exposition," *Control and Dynamic Systems*, edited by C. T. Leondes, Vol. 16, Academic Press, New York, 1980, pp. 81–129.

[10]Burken, J. J., Lu, P., Wu, Z., and Bahm, C., "Two Reconfigurable Flight Control Design Methods: Robust Servomechanism and Control Allocation," *Journal of Guidance, Control, and Dynamics*, Vol. 24, No. 3, 2001, pp. 482–493.

[11]Hanson, J., "Advanced Guidance and Control Project for Reusable Launch Vehicles," AIAA Paper 2000-3957, Aug. 2000.

[12]Justus, C. G., and Johnson, D. L., "The NASA/MSFC Global Reference Atmospheric Model: 1999 Version (GRAM-99)," NASA TM-209630, May 1999.

[13]Cobleigh, B. R., *Development of the X-33 Aerodynamic Uncertainty Model*, NASA TP-1998-206544, Apr. 1998.